Bull. Astr. Soc. India (2000) **28**, 687-695

NIFS : A Near Infrared Imaging Fabry-Perot Spectrometer

B.G. Anandarao, M.S. Nanda Kumar, N.S. Jog and R.T. Patel

Physical Research Laboratory, Ahmedabad 380 009, India.

Received 7 March 2000; accepted 10 October 2000

Abstract. We describe here a Near-Infrared Imaging Fabry-Perot Spectrometer (*NIFS*) operating in the *K* band to provide a maximum spectral resolution of 2000-3000 over two optional fields of view of ~ 2′ x 2′ and 4′ x 4′ with plate scales of 0.5″ and 1″ / pixel respectively. *N I F S* is an add-on instrument to an existing infrared camera with a 256x256 *HgCdTe* array detector. The instrument is operational with a 1.2 m telescope to primarily work on star forming regions and starburst galaxies which strongly emit in several diagnostically important lines within the *K* band. The design, testing and operation of *NIFS* are discussed in the light of preliminary observations made on the Orion Molecular Cloud Complex.

Key Words : techniques : spectroscopic, instrumentation : spectrographs, infrared : general.

1. Introduction

The technique of imaging Fabry-Perot Spectrometry (*FPS*) is proven to be one of the most powerful tools for velocity mapping of extended astronomical sources (Atherton et al. 1982; Bland & Tully 1989; Seema et al. 1992). While the technique has been in use for the optical region since a long time, its utilization in the infrared region is relatively recent (Krabbe et al. 1993; Luhman et al. 1995; Ryder et al. 1998). Star forming regions (particularly the low mass star forming regions) emit weakly in optical wavelengths. However, they are the strongest emitters in the near-infrared region which makes it possible to carry out imaging spectroscopy of these objects even with a 1-2 m class telescope. Kinematics of star forming regions is one of the most important studies of current interest. The technique helps in understanding the energetics of the outflows and other manifestations of star formation. Recently we have constructed an imaging *FPS* in the near-infrared (*NIR*) to be used at the *f*/13 cassegrain focus of the 1.2 m Gurushikhar Infrared Telescope (*GIRT*) facility at Mt. Abu, W. India. This paper describes the details of its optics, its performance and some preliminary results on the Orion Molecular Cloud - 1 (OMC1) region. The *FPS* works at a maximum resolving power of 3000 in the region 2-2.5 μm (*K* band) and utilizes a 256x256 *HgCdTe* array camera as the detector.

2. Telecentric mode vs classical mode

The *FPS* can in principle be used in a variety of configurations for imaging spectroscopy (Meaburn 1976). In the conventional mode a collimated beam is used to project the interference fringes on an array detector by means of an imaging lens. In the telecentric mode the *FP* etalon is inserted into the converging beam of the telescope (as shown in Fig 1) and images are obtained for several etalon gap settings covering one free spectral range (*FSR*). Since the fringe system forms at infinity, one does not see it like in the classical mode but one sees instead an image at the resonant wavelength decided by the gap of the etalon. Another important difference between the two modes is in the maximum available resolving power of the spectrometer. In the case of telecentric mode, this factor is directly dependent on the f-ratio of the converging beam of the telescope, given by the formula

$$\frac{\theta^2}{8} = \frac{1}{R} \tag{1}$$

where θ is the full cone angle of the incident beam which is called the acceptance angle and the f-number is simply its inverse. From this we get a relationship between the resolving power and the f-number as

$$R = \frac{8}{\pi} \times (f - number)^2 \tag{2}$$

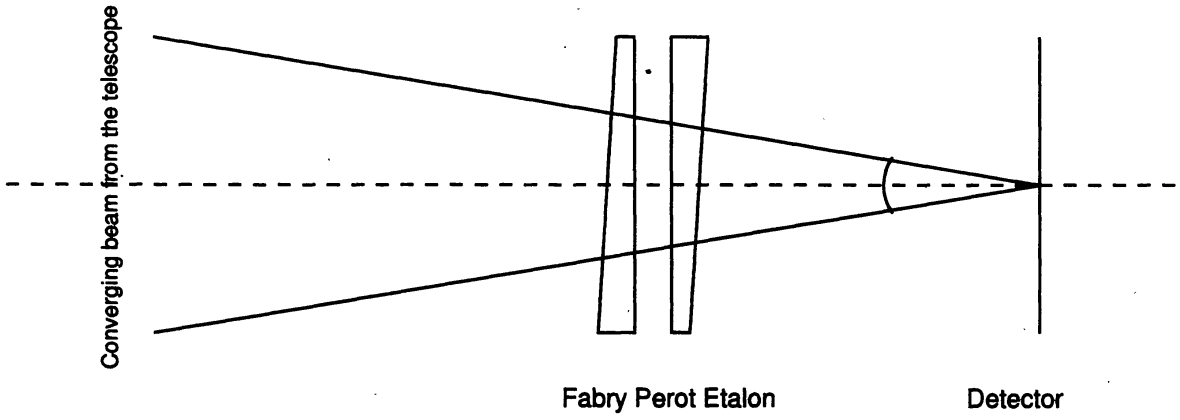

Figure 1. Schematic representation of the Telecentric mode of operation of the Fabry-Perot Etalon.

In the classical mode the resolving power of the *FP* is decided by the acceptance cone at the detector formed by the imaging lens. In either case, it is the endeavor of the experimenter to see that the maximum possible resolving power for a given etalon is preserved. However, while operating at R ~ 3000-5000, the loss in the resolving power due to the usage of a converging beam, of say, *f*/13 ratio, is marginal in comparison with the classical way of using the collimated beam (see Atherton et al. 1982).

The main concern in imaging spectroscopic observations is to obtain a reasonable *S/N* ratio over the required spectral coverage. In the classical mode of operating the *FP*, the etalon needs to be scanned by changing the cavity gap to cover the entire spatial extent of an extended source. As the gap is changed in suitable steps, the diameter of the fringes keeps changing covering the spatial extent in its entirety. The intensity variation on a single pixel (corresponding to a particular spatial position) will constitute the line profile at that location. The intensity variation with the scanning step depends upon the pixel position due to the non-linearity of the variation of wavelength λ with the angle of incidence θ. For any pixel (x, y), the deviation from the central pixel wavelength (say, λ_o) is given by :

$$\delta\lambda_{x,y} = \lambda_o(1 - \cos\theta) \tag{3}$$

and this variation or 'the phase map' can then be obtained by using a standard laboratory source. During observations at the telescope, this calls for obtaining images at 40 steps (gap settings) of the *FP* (for a finesse of say 20) to cover one *FSR*. Given the problems of large sky background in the *K* band, that requires sky subtraction for every frame, the time factor gets atleast doubled which makes the procedure equivalent to obtaining images at 80 steps.

In the telecentric mode, since the image is formed by the converging beam directly on the array, one can dispense with the statutory phase correction. Hence, it suffices to obtain images only at 5-10 steps around the spectral line of interest to which the *FP* is tuned (see section 5). This infact gives better than the Nyquist sampling on the spectral line. Considering the sky subtraction factor, the total time required to obtain images at 10-20 steps works out to be a factor of 5 smaller than the classical mode. It is therefore highly advantageous to use the telecentric mode in the infrared region at nominal resolutions. Another important advantages of the telecentric mode is the relatively simple data reduction procedure that can be carried out using regular *CCD* processing routines in the astronomical image processing softwares like *IRAS* or *MIDAS*. Analysis of the data obtained in the classical mode requires specially written software packages like the one used for *TAURUS* (Atherton et al. 1982).

Furthermore, in the case of the classical setup the light loss is considerable due to the usage of two lenses, one for collimation and the other for imaging which may even cause a possible image distortion.

3. Optics

Figure 2 shows a schematic of the optical set-up of the *NIFS*. The *f*/13 beam from the 1.2 m *GIRT* passes through a piezo-electrically scanned servo-controlled *FP* etalon (Queensgate, UK) of usable aperture of 50 mm and a cavity gap of 100 μm (see Table 1 for features). The

beam is then passed through the dewar window via a 45° mirror into the liquid nitrogen cooled dewar. The *FP* etalon is kept at room temperature as near to the dewar window as possible to reduce the stray radiation noise. The background contribution is about a factor of $\sqrt{2}$ or so higher for a warm *FP* etalon kept close to the detector dewar than for a cooled etalon (Persson et al. 1982). The telescope *f*/13 beam is focused on the aperture after passing through the filter wheel that contains narrowband filters used for order-sorting. Table 2 lists the set of order-sorting filters available with *NIFS*. The camera is *NICMOS*-based and contains a grating spectrograph of resolving power 1000. In principle, the *F P* etalon can be used directly in the imaging mode with the narrowband filters which serve the purpose of order-sorting or it can be used in conjunction with the grating spectrograph. Each pixel on the 256 x 256 array detector corresponds to a sky angle of 1.0″ or 0.5″ depending upon whether the focal reducer lens is in the beam or out of the beam. The design of the etalon mount is made in such a way that it can be inserted in the instrument when intended. A provision is also made for using the *FP* in the classical mode by means of the optical lenses as shown in Fig 2 especially for point sources.

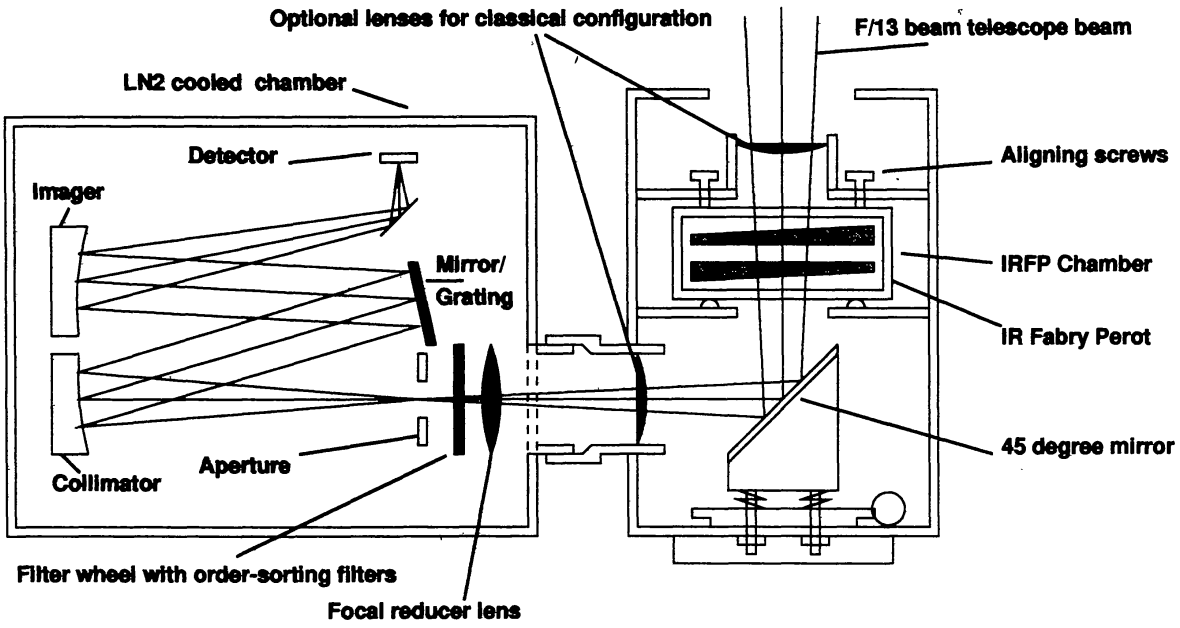

Figure 2. Schematic Diagram of the optical layout of the NIFS.

4. Scanning the Etalon

The scanning of the *FP* etalon is done by the computer generated pulses fed through an *RS*232 interface into the servo-control system *CS* 100 (Queensgate, UK). The scanning step size and the scanning length can be chosen through the computer. At each step of the scanning the signal can be integrated for an appropriately specified time. A standard Krypton laboratory source was used to obtain the images (the KrI 2.19 μm line). Typically a total of 135 steps of scanning are required to cover one *FSR* which is 0.0225 μm at 2.121 μm for the present case. Each such step effects a gap change of 1.67×10^{-4} μm corresponding to a Doppler velocity resolution element of 23.6 km/s. The *FWHM* of the instrumental function was measured to

Table 1. *NIFS* Characteristics

Quoted Values	
Usable aperture	50 mm
Wavelength range	2 - 2.5 μm
Reflectivity	95%
Free spectral range (FSR)	0.02 μm (3000 km/s)
Resolving power ($\lambda/\delta\lambda$)	5000
Velocity resolution ($\delta\upsilon$)	60 km/s
Resolution ($\delta\lambda$)	4×10^{-4} μm
Determined Values	Telecentric mode *f*/13 beam
Free spectral range (FSR)	0.0225μm (~3000km/s)
Instrument FWHM ($\delta\lambda$)	0.0014 μm (212 km/s)
Finesse	16
Resolving power ($\lambda/\delta\lambda$)	2500-3000
Velocity resolution ($\delta\upsilon$)	90 km/s

be $\delta\lambda$ = 0.0014 μm or 212 km/s in Doppler velocity having a sampling of 9 steps. A finesse of 16 has been realised with this mode of operation. At the order of interference of about 100 (at 2 μm), we get a nominal resolving power of 1600. However, using gussian decomposition techniques, it is possible to resolve features separated by around 90 km/s in cases of high *S/N* ratios. This gives a resolving power of about 2500-3000.

5. Parallelism and tuning adjustments

The *FP* needs to be adjusted for parallelism before inserting into its chamber. Although the parallelism adjustments are made by using pre-determined standard *CS* 100 settings, it is possible to make a quick confirmatory test before starting the night observations. A simple technique by which one can adjust the parallelism to a very good accuracy is by visually looking at the fringes. For a perfectly parallel etalon, the fringe pattern remains steady when one scans with the eye across the etalon face in two orthogonal directions. Although *IRFP*'s are almost opaque for optical wavelengths, a narrow band of good reflectivity exists for the coatings allowing us to use a helium arc lamp (preferable) or a *He – Ne* Laser (diffused by a screen) for parallelism adjustment.

Table 2. List of *NIFS* order-sorting filters

Filter	λ_{max} (μm)	$\Delta\lambda(\mu m)$
H_2 S(1)	2.118	0.043
NB1	2.135	0.043
Brγ	2.165	0.044
NB2	2.217	0.083
CO	2.373	0.101

Once the emission line of interest is chosen, the appropriate pre-filter should be brought to position inside the camera and the *FP* has to be tuned to the line of interest. It is customary to adjust the CS100 z dial settings to the standard laboratory pre-determined values. We have found that this laboratory calibration has remained stable to an accuracy of less than one step in more than 3 mounths. However, in cases where the z values for tuning are not established or doubtful, we have devised the following method. The telescope is aimed at the flat-field screen illuminated with a Krypton lamp (for the KrI line at 2.19 μm) and the *FP* is scanned until the Krypton line intensity maximises. This can be done by setting the camera into movie mode (continuous display) and monitoring the mean counts of the frames. The *C S* 100 z setting position for the desired wavelength can be found by using pre-established relation between the z-positions for the Krypton line peak and for any other desired wavelength. A short cut to this procedure is possible using bright molecular envelopes of planetary nebula or molecular cloud regions like the OMC-1 available in the sky during observations. For example, the z value for which the emission line peaks can be determined for common emission lines like H_2, Brγ in less than 2-3 minutes with a 1.2 m telescope using the OMC-1.

6. Observations and data analysis

Once the *FP* is turned to an appropriate line, it is required to obtain images at different gap settings of the *FP*, spaced equally around the line. Although a minimum of 4 steps will suffice the purpose, the choice of the total number of steps is left to the observer and depends on the type of the object. An object and a sky frame has to be obtained for each *FP* setting. The median combined sky frames at each *FP* setting form the respective flat frames. The data is reduced using standard *CCD* processing routines like *CCDROC* of *IRAF*. Reducing the frames at each *FP* setting will result in a stack of images that form a data cube. The stack of images forms the spectral dimension and pixel-to-pixel intensity variation across this stack gives a spectral line profile.

Preliminary observations were carried out during several clear nights in Jan 1999 using the 1.2 m Infrared Telescope Facility (*GIRT*) at Mt. Abu. We selected the region of the OMC-1 since it has been one of the most well-studied objects and our results can be compared with those of the earlier authors. The region covered by the array was approximately 4′ x 4′. For comparison, narrowband (2%) filter images of the molecular hydrogen emission ($v = 1 - 0S(1)$ at 2.121 μm) around a region approximately 4′ x 4′ were also taken and a mosaic of such images is presented in Fig 3. This image of approximately 8′ x 8′ in extent, may be compared

Figure 3. A mosaic of four narrowband images of 4′ x 4′ around the Orion Molecular Cloud 1 Complex showing the molecular hydrogen emission regions along with the continuum. The image size is approximately 8′ x 8′. One can identify various features of the complex such as the Trapezium stars, the Orion Bar ionization front, and the inumerable number of embedded stars.

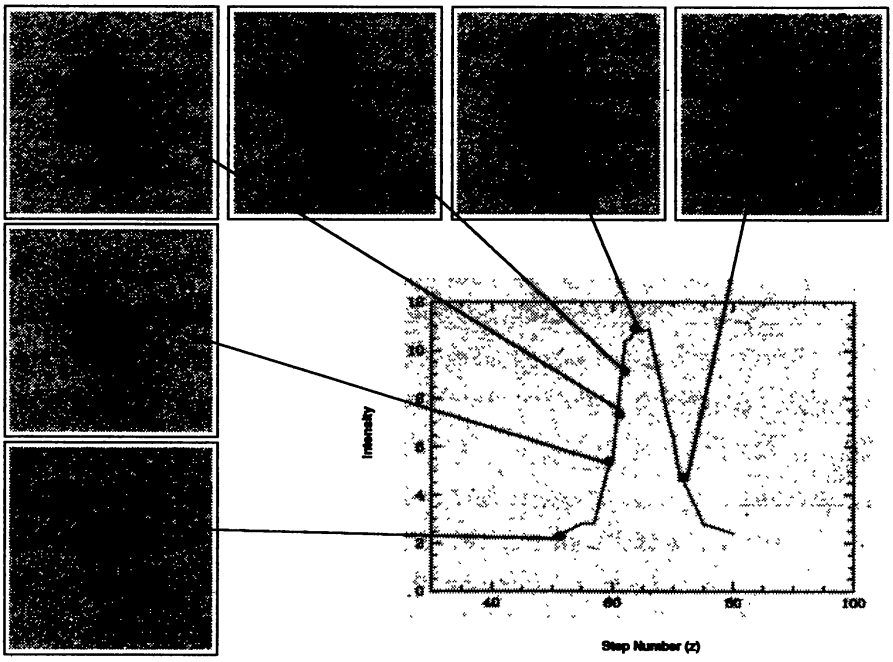

Figure 4. Images of the Orion nebula at different scanning steps around the Molecular Hydrogen emission line at 2.121 μm.

and calibrated with the images taken in the photometric survey conducted by McCaughrean & Stauffer (1994). This image is not continuum-subtracted and hence does not represent pure emission line regions. On the other hand the FP images shown in Fig 4 represent the Orion complex at different steps of the etalon gap giving a more accurate depiction of emitting regions in a much narrower bandwidth. One can notice the brightening of the nebular matter emitting the $\nu = 1 - 0S(1)$ vibrational transition of molecular hydrogen at 2.121 μm as the etalon gets gradually tuned by the process of scanning. We estimate a finesse of 16 once again confirming our result obtained with the laboratory standard spectral source. One can notice from Fig 4 a very dynamic pattern of emission indicating the disruption of the parent molecular cloud. The molecular hydrogen emission is extended over several square arcminutes and includes the BN object, the KL nebula and several infrared point sources indentified by Beckwith et al. (1978) as well as IRAS. These results are morphologically in good agreement with those obtained by Schild et al. (1997). The emission appears to be highly filamentary (see the northern region) and clumpy. Schild et al. (1997) proposed that such "linear structures" could be due to molecular matter swept up into the jet from the surrounding regions. These are thought to be density rather than temperature variations. Chakraborty & Anandarao (1999) interpreted the observed velocity variations as due to the corresponding density fluctuations in the case of the Hourglass HII region in the Lagoon Nebula. Therefore the spatially resolved velocity observations are very important to be made in the infrared emission lines. We determine a 3σ limit, for the NIFS at the 1.2m telescope, of 1×10^{-17} watts/m^2/arcsec^2 for an integration time of 40 sec on the peak of the molecular hydrogen emission line.

The NICMOS camera has two fields of view, $2' \times 2'$ and $4' \times 4'$. The larger field is obtained by introducing a converging lens (a simple doublet) into the beam (inside the dewar). This lens is found to give distorted images outside a circle of diameter of about $3'$. The NICMOS images of smaller field (i.e., without the extra lens) are mostly distortion free. The FP etalon does not introduce any distoritions but ghosts can be there. The ghosts were avoided by slightly tilting the etalon. In Figs 3 and 4, one can notice in many places, stars whose images are circular (this was ascertained by taking a linear scan or a contour envelope of the images). Some stars appear elongated due to the overlap with a fainter star in the line of sight (for example, near the Trapezium stars). This was verified against the high (spatial) resolution images of McCaughrean & Stauffer (1994) which agree with our images.

7. *NIFS* as tunable filter for emission line imaging

The near-*IR* molecular hydrogen emission lines are recognised as being important tools in studies of star formation (Shull & Beckwith 1989). The ratio of intensities of these lines arising from transitions from different vibrational levels can be used to identify the mechanism of excitation. A knowledge of the mechanism would in turn throw light on the energetics involved in the regions of recent star formation. The spectrophotometric imaging technique can be exploited to map regions in two or more lines and from the ratio of the maps one can delineate the shocked and the *UV* fluorescing regions. Narrowband images in H_2 and Brγ can reveal the atomic and molecular hydrogen distribution in the star forming regions. Thus, in addition to being a moderate resolution spectrometer, one can use *NIFS* as a tunable filter of very narrow bandwidth with *FWHM* ($\approx 0.0014\mu$m) to image regions of star formation in emission lines of

astrophysical interest. It is required to obtain two images in order to obtain a narrowband image: one image with the *FP* tuned to the on-line wavelength and another by detuning the *FP* to an off-line wavelength. The difference image results in a continuum-subtracted line image. Continuum subtraction is otherwise a difficult and relatively inaccurate procedure while doing with conventional narrowband filters. But the Fabry-Perot technique gives a perfect way of subtracting the continuum and has great advantages while imaging the close environments of young stars where the regions of interest are highly contaminated by the continuum emission from the star. This technique is also useful while studying jets that are seen tracing all the way upto the stellar seeing disk. NIFS can be used to image high-mass star forming regions with significantly reduced contamination from the intense continuum emitting sources. Further, the technique can be used for making accurate observations of galaxies with closely spaced adjacent redshifts.

Acknowledgements

This work is supported by the Department of Space, Government of India. We thank A.J. Shroff, J.A. Panchal and A. Panchal for help in mechanical work. We thank J.N. Desai for supporting the project.

References

Atherton P.D., Reay N.K., Ring J., Hicks T.R., 1981, Opt. Engg., 20, 806.

Atherton P.D., Taylor K., Pike C.D., Harmer C.F.W., Parker N.M., Hook R.N., 1982, MNRAS, 201, 661.

Beckwith S., Persson S.E., Neugebauer G., Becklin E.E., 1978, ApJ, 223, 464

Bland J., Tully B., 1989, AJ, 98, 723.

Chakraborty A., Anandarao B.G., 1999, A&A, 346, 947.

Krabbe A., Rotaciuc V., Storey J.W.V., Cameron M., Blietz M., Drapatz S., Hofmann R., Samann G., Genzel R., 1993, PASP, 105, 1472

Luhman M.L., Jaffe D.T., Keller L.D., Pak S., 1995, 107, 184

McCaughrean M.J., Stauffer J.R., 1994, AJ, 108, 1382

Meaburn J., 1976, Detection and Spectrometry of Faint Light (Dodrecht, Reidel).

Nandakumar M.S., 1999, Thesis, Gujarat University.

Persson S.E., Geballe T.R., Baas F., 1982, PASP, 94, 381.

Ryder S.D., Ashley M.C.B., Sun Y.S., Burton M.G., Allen L.E., Storey J.W.V., 1998, PASA, 15, 228

Schild H., Miller S., Tennyson J., 1997, A&A, 318, 608.

Shull J.M., Beckwith S., 1982, ARA&A, 20, 163.

Seema P., Anandarao B.G., Banerjee D.P.K., Jog N.S., Patel R.T., 1992, PASP, 104, 1091.